Int J Adv Manuf Technol (2013) 64:1057–1072
DOI 10.1007/s00170-012-4053-z

ORIGINAL ARTICLE

Genetic algorithm-based numerical optimization of powder compaction process with temperature-dependent cap plasticity model

Sh. Keshavarz · A. R. Khoei · Z. Molaeinia

Received: 11 October 2011 / Accepted: 5 March 2012 / Published online: 25 March 2012

Abstract In this paper, a shape optimization technique is presented for the cold and hot isostatic pressing of metal powders based on the genetic algorithm (GA) approach. The GA technique is used to obtain the desired optimal compacted component by changing the boundaries of component and verifying the prescribed constraints. The coupled thermomechanical analysis of hot isostatic pressing is employed for metal powders during densification process. The numerical modeling of hot powder compaction simulation is performed based on the large deformation formulation, temperature-dependent cap plasticity model, and frictional contact algorithm. The modified cap plasticity takes the temperature effects into the numerical simulation of highly nonlinear behavior of metal powder. Finally, numerical examples are analyzed to demonstrate the feasibility of proposed optimization algorithm for designing powder components in the cold- and hot-forming processes of powder compaction.

Keywords Hot powder compaction · Shape optimization · Genetic algorithm · Modified cap plasticity · Large deformation

1 Introduction

Powder compaction is one of the most important processing procedures in the manufacturing industry, which changes the shape and characteristics of powder through the plastic deformation without any removal of material during the process. A major advance in powder metallurgy technology has been the warm compaction process, which can utilize traditional powder compaction equipment. This method is applicable to most powder material systems but requires that both the powder and the die assembly are heated up to a temperature in the range of $0.6T_m$, where T_m is the melting temperature of the metal composing the powder. It is important to obtain the HIP products with near net shape geometry in order to reduce costs for extra machining, especially for less machine able materials. However, it is well-known that the final geometry of the products differs from that desired not only in the shape but also in scale. This is due to container stiffness and temperature gradients during the densification process. Hence, it is essential to be able to forecast the behavior of the powder and container under the HIP process in order to predict the final shape of the product. The aim of this study is to develop an optimization methodology through the finite element (FE) simulation of hot powder compaction process.

In order to develop an optimization algorithm for hot powder forming process, the genetic algorithm technique is employed into the nonlinear large FE deformation. The goal of the optimization is to eliminate the workpiece defects that may arise during the powder compaction process. The genetic algorithm is used since it is suitable for discrete or continuous variables, the derivative information is not required, a wide sampling of domain can be searched simultaneously, a list of optimal parameters can be provided, and all kinds of data, such as numerical data, experimental data, or analytical functions, can be employed [1]. The objective function of the optimization algorithm is associated with the quality of the final product. The GA technique is used to increase the efficiency of the search algorithm and to design the optimal preform design of compacted component.

S. Keshavarz · A. R. Khoei (✉) · Z. Molaeinia
Center of Excellence in Structures and Earthquake Engineering, Department of Civil Engineering, Sharif University of Technology, P.O. Box. 11365-9313, Tehran, Iran
e-mail: arkhoei@sharif.edu

In powder metallurgy, numerical modeling of cold compaction process of powder die pressing has been extensively developed to control the properties of final product, including the large deformations of powder compaction by Khoei and Lewis [2], the powder plasticity behavior by Haggblad and Oldenburg [3] and Brandt and Nilsson [4], and the contact friction between the powder and tools by Keshavarz et al. [5]. In hot powder pressing, the densification behavior of powder was studied by Jinka and Lewis [6] and Svoboda et al. [7] based on the modification of plasticity theory of porous solids. Various forming processes of hot working have been simulated by means of the finite element method during last decades; however, most simulations have dealt with incompressible, or slightly compressible material models which keep volume constant during the plastic deformation [8]. In this study, the nonlinear behavior of hot powder is described using a temperature-dependent cap plasticity model. The modified cap plasticity model is employed to capture the major features of the response of initially loose metal powders to complex deformation histories which are encountered in the hot compaction of powder component. In order to perform the numerical modeling of hot powder compaction simulation, the modified cap plasticity model together with the frictional contact algorithm is employed into the thermomechanical analysis of large FE deformation. Finally, in order to perform the shape optimization of hot powder compaction process, the optimal design algorithm recently proposed by Khoei et al. [9] in the cold forming process is extended to the hot powder die pressing based on the coupled thermomechanical FE simulation in the framework of genetic algorithm technique.

The plan of the paper is as follows: In Section 2, an overview of shape optimization technique is presented for hot compaction of powder die pressing. The genetic algorithm is described to obtain the desired optimal compacted component by changing the boundaries of component and verifying the prescribed constraints. In Section 3, the numerical modeling of thermomechanical FE simulation is presented in the framework of a large deformation FE formulation and the heat transfer analysis. In Section 4, the powder plasticity behavior is described based on the temperature-dependent cap plasticity model. In Section 5, the numerical simulation of the complicated die geometry is presented to evaluate the capability of the GA in shape optimization of hot powder compaction process. Finally, some concluding remarks are given in Section 6.

2 Optimal design technique

The optimal design method consists of the essential ingredients, including the shape generation and control, mesh generation, nonlinear finite element analysis, sensitivity analysis, and design optimization. In order to make an optimal design, we need to define the basic characteristics of the final product that need to be optimized. These features may be the shape or topological configuration. The optimization methods include mathematical optimization, backward tracing, artificial intelligence, experiment optimization, and automatic control algorithm [10]. There are several optimization algorithms presented by Antonio and Dourado [11] and Sousa et al. [12] for metal forming processes, such as the simplex optimization algorithm, the genetic optimization algorithm, an inverse revolutionary search algorithm, and the gradient-based optimization algorithm.

The optimization process can be divided into three main tasks [13]. The first step is to define the geometric and analytical model. In geometric model, the design variables are easily imposed, and it allows an explicit integration with other design tools. The analytical model is used to obtain the structural response of the system subjected to external actions. The next step includes a sensitivity analysis to obtain a solution of the problem. Finally, an appropriate optimization algorithm needs to be performed to solve the problem in an effective and reliable way. The search of a robust optimization algorithm is necessary to survive in different environments. In this study, the genetic algorithm is employed due to the fact that it is theoretically and empirically proven to provide a robust search in complex space.

2.1 Genetic algorithm technique

A genetic algorithm comprises four main operations: fitness selection, crossover, elimination/substitution, and mutation [14]. It starts from an initial population representing possible solutions of the problem. From these operators, crossover and mutation are applied to the population in improving the objective function value to form the new generation, in which the members have higher quality. Each member in the population corresponds to a solution in the solution space. The quality of a member is represented by its fitness associated with the objective function value. The principle of survival of the fittest is taken as a rule in the search process. Mutation models random change in the genetic information of creatures and is inspired by random change of genetic information in living organisms. Crossover models the exchange of genetic information of creatures and is inspired by exchange of genetic information in living organisms. Fitness selection models reproductive success of adapted organisms in their environment.

The first step in the implementation of genetic algorithm is to generate an initial population. In genetic algorithm, each member of population has a binary string, referred as a genotype, or a chromosome. In most cases, the initial population is generated randomly. After creating an initial population, each string is evaluated and assigned a fitness value. The notion of evaluation and fitness are sometimes used interchangeably. However, it is useful to distinguish between the evaluation

function and the fitness function used by a genetic algorithm. Here, the evaluation function, or objective function, provides a measure of performance with respect to a particular set of parameters. The fitness function transforms that measure of performance into an allocation of reproductive opportunities. The fitness can be assigned based on a string rank in the population, or by sampling method, such as tournament selection. It is helpful to view the execution of the genetic algorithm as a two-stage process [15]. It starts with the current population. Selection is applied to the current population to create an intermediate population. The recombination and mutation are then applied to the intermediate population to create the next population. The process of going from the current population to the next population constitutes one generation in the execution of a genetic algorithm. In genetic algorithm, the probability that strings in the current population are duplicated and placed in the intermediate generation is proportion to their fitness. The operators are applied in the following sequence [16, 17]:

Initialization A random generation of initial population is generated.

Selection This operator ranks the population according to the solution fitness. The selection operator is randomly made with an equal probability distribution for each solution. The two selection processes are independent and the based-fitness probability is considered to select each one of the parents.

Crossover This operator generates the offspring population using couples of parents chosen with the selection operator. The crossover transforms two chromosomes (progenitors) into a new chromosome (offspring) having genes from both progenitors. The crossover is applied with a predefined probability to the genetic material of the highest fitted chromosome.

Elimination/ substitution This operator is applied to control the genetic similarity between individuals of the population created by the crossover. The enlarged population is ranked according to their fitness and elimination of solutions with similar genetic properties and consequent substitution by new randomly generated individuals.

Mutation The mutation operator is used to overcome the problem induced by selection and crossover operators where some generated solutions have a large percentage of equal genetic material. The mutation makes possible the exploration of previously unmapped space design regions and guarantees the diversity of the generated population.

Stopping criterion The stopping criterion used in the convergence analysis is based on the relative variation of the mean fitness of a reference group during a fixed number of generations and the feasibility of the corresponding solutions. If the constraints of the problem are not satisfied, then the evolutionary process continues.

2.2 Implementation of GA technique

In hot forming of metal powder, we optimize the process in different ways depending on various criteria, such as precise shape, die filling, friction coefficient, punch forces, or uniform distribution of mechanical properties. An optimal design criterion frequently encountered in powder die pressing is the shape optimization to achieve the precise forming of finished component shape. Consider that we need to determine the optimal shape of preform workpiece at final compaction process, the geometry of the preform workpiece is considered as unknown design variables. The optimization algorithm is implemented to optimize the difference between the maximum and minimum values of stress on the final compacted component with the objective function defined as

$$\text{Minimize} \quad f(x) = |\sigma_{\max} - \sigma_{\min}| \tag{1}$$

where x denotes the design variable vector and the constraints $c_i(x) \geq 0$, $i = 1, 2, \ldots, n$ are used to control the geometry of component. After identifying the design variables and search domain that represents the population phenotype, different solutions are represented by an appropriate code format called the genotype. The establishment of a code format is the main step of GA formulation. Here, a binary code is developed with different number of bits for each design variable. The technique is performed by an initial population generated randomly using strings based on the design variable vector x. The numerical simulation is carried out for each string to calculate the fitness and reproduction. The process of reproduction is applied according to the value of objective function obtained at the end of compaction to copy the individual string. The reproduction operator is implemented in the algorithmic form based on a roulette wheel where each individual is represented by a space that proportionally corresponds to its fitness.

The genetic algorithm described above generates a sequence of parameters to be tested using the system model, objective function, and the constraints. The genetic algorithm technique is employed to search the unconstrained objective functions. However, there are one or more constraints in powder compaction problems that need to be satisfied. Constraints are generally classified into equality, or inequality relations. Since equality constraints are subsumed into a system model, we deal with inequality constraints. We must evaluate the objective

function and check if any constraints are violated. If not, the parameter set is assigned the fitness value corresponding to the objective function evaluation. If constraints are violated, the solution is infeasible and thus has no fitness. As a result, we obtain information out of infeasible solutions by degrading their fitness ranking in relation to the degree of constraint violation, which is called as the penalty method. In this procedure, a constrained problem in optimization is transformed to an unconstrained problem by associating a cost, or penalty with all constraint violations. This cost is included in the objective function evaluation (Eq. 1) and can be therefore transformed to the unconstrained form as

$$\text{Minimize} \quad f(x) + r\sum_{i=1}^{n}\phi[c_i(x)] \tag{2}$$

where ϕ and r are the penalty function and penalty coefficient, in which a number of alternatives exists for the penalty function ϕ. It must be noted that the implementation of an integrated genetic software into a highly nonlinear simulation, such as hot compaction of powder die pressing, plays an important role, since the nonlinear analysis cannot be restarted from the initial boundary condition due to large deformations and highly nonlinear material behavior. Here, an integrated genetic software is incorporated into a nonlinear FE code together with an automatic mesh generator to make the process of optimal design more efficient.

3 Nonlinear thermomechanical finite element modeling

3.1 Large deformation FE formulation

In nonlinear elastoplastic analyses, whether the displacements, or strains, are large or small, it is imperative that the equilibrium conditions between the internal and external forces are satisfied. A general description of strains was introduced by Green and St. Venant, in which the nonlinear strain displacement relationship can be defined in terms of the infinitesimal and large displacement components. In order to develop a finite element formulation, the FE Galerkin discretization can be applied to the nonlinear elastoplastic equilibrium equation. Following the standard finite element procedure, the initial domain Ω is divided into elements. If the displacements within an element are prescribed by a finite number of nodal values with the independent approximations of $\mathbf{u}$ defined as $\mathbf{u} = \mathbf{N}\overline{\mathbf{u}}$, the finite element formulation can be written as [18]

$$\int_{\Omega}\overline{\mathbf{B}}^{T}\mathbf{S}\; d\,\Omega - \mathbf{f} = 0 \tag{3}$$

where $\mathbf{S}$ is the second Piola–Kirchhoff stress and the matrix $\overline{\mathbf{B}}$ is the well-known strain matrix relating the increments of strain and displacement, in which for large deformation it contains the higher order displacement derivatives [18]. In order to obtain the tangential stiffness matrix $\overline{\mathbf{K}}_T$, the FE Galerkin discretization formulation (Eq. 3) can be appropriately taken variations with respect to $\mathrm{d}\overline{\mathbf{u}}$. The stiffness matrix $\overline{\mathbf{K}}_T$ consists of two parts: The first part involves the derivative of stress $\mathrm{d}\mathbf{S}$, which depends on the material response and leads to the material tangent stiffness matrix $\mathbf{K}^{\mathrm{mat}}$, and the second part involves the current state of stress $\mathbf{S}$, which accounts for the geometric effects of the deformation (including rotation and stretching) and leads to the geometric stiffness matrix $\mathbf{K}^{\mathrm{geo}}$. To derive the material tangent stiffness matrix $\mathbf{K}^{\mathrm{mat}}$, the constitutive law can be implemented with respect to the incremental second Piola–Kirchhoff stress, i.e., $\mathrm{d}\mathbf{S} = \mathbf{D}_S^{\mathrm{ep}}\mathrm{d}\,\mathbf{E}$, as

$$\mathbf{K}^{\mathrm{mat}} = \int_{\Omega}\overline{\mathbf{B}}^{T}\mathbf{D}_{\mathrm{S}}^{\mathrm{ep}}\overline{\mathbf{B}}\; d\,\Omega \tag{4}$$

The geometric stiffness matrix $\mathbf{K}^{\mathrm{geo}}$ can be defined as

$$\mathbf{K}^{\mathrm{geo}} = \int_{\Omega}\mathbf{G}^{T}\mathbf{M}_{\mathrm{S}}\mathbf{G}\, d\,\Omega \tag{5}$$

where $\mathbf{M}_{\mathrm{s}}$ is a 4×4 matrix of the three PK2 stress components. All the ingredients necessary for computing large deformation problems are now available. For each iterations, $\left(\overline{\mathbf{K}}_T\right)_n$ is obtained. The Cauchy stress $\boldsymbol{\sigma}$ is calculated based on the PK2 stress using $\boldsymbol{\sigma}=J^{-1}\mathbf{F}\;\mathbf{S}\;\mathbf{F}^{T}$, with J denoting the determinant of $\mathbf{F}$, i.e., $J=\det(\mathbf{F})$.

3.2 Heat transfer FE formulation

In order to derive the thermomechanical finite element formulation, the Lagrangian finite element technique, presented in previous section, is incorporated into the heat transfer formulation. The governing equation of heat conduction is derived for a continuous medium from the principle of conservation of heat energy over an arbitrary fixed volume. Based on this principle, the heat increase rate of the system is equal to the summation of heat conduction rate and heat generation rate in a fixed volume. In order to solve the heat conduction equation, the standard finite element Galerkin discretization process is used by approximating the temperature field T as $T = \mathbf{N}\overline{\mathbf{T}}$, where $\mathbf{N}$ is the shape function and $\overline{\mathbf{T}}$ is the nodal temperature. Applying the FE Galerkin discretization into the heat conduction equation, it results in

$$\mathbf{C}\,\dot{\overline{\mathbf{T}}} + \mathbf{H}\overline{\mathbf{T}} = \mathbf{G} \tag{6}$$

where the capacity matrix $\mathbf{C}$, the conductivity matrix $\mathbf{H}$, and the thermal loading vector $\mathbf{G}$ are defined as

$$\begin{aligned}\mathbf{C} &= \textstyle\int_{\Omega}\mathbf{N}^{T}\rho c\mathbf{N}d\Omega\\ \mathbf{H} &= \textstyle\int_{\Omega}\mathbf{B}^{T}\boldsymbol{k}\mathbf{B}d\Omega + \int_{\Gamma_\alpha}\mathbf{N}^{T}\alpha\mathbf{N}d\Gamma_\alpha\\ \mathbf{G} &= \textstyle\int_{\Omega}\mathbf{N}^{T}Qd\Omega - \int_{\Gamma_{\mathbf{q}}}\mathbf{N}^{T}q\mathrm{d}\Gamma_{\mathbf{q}} + \int_{\Gamma_\alpha}\mathbf{N}^{T}\alpha T_a d\Gamma_\alpha\end{aligned} \tag{7}$$

where c is the specific heat capacity; Q the heat generation rate of the system; k the thermal conductivity matrix; q and Γ_q are the heat flux and the surface boundary of heat flux, respectively; α and Γ_α are the convection heat transfer coefficient and the surface boundary of heat transfer, respectively; and T_a is the atmospheric temperature.

In order to discretize the FE equation of heat conduction (Eq. 6) in time, the time stepping procedure is employed based on the θ method, i.e., $T_{n+\theta}=\theta T_{n+1}+(1-\theta)T_n$. In the basis of heat conduction finite element equation, the distribution of temperature can be achieved at each time interval. The thermal expansion/contraction strain $\Delta\varepsilon$ due to changes of temperature can then be obtained by using $\Delta\varepsilon=\alpha_T\Delta T$, with α_T denoting the thermal coefficient. The value of thermal strain can be calculated at each quadrature point and used as the external forces in the nonlinear finite element analysis. Finally, the stress and density distribution can be evaluated using the nonlinear large deformation FE model.

3.3 Thermomechanical FE simulation

In order to perform the coupled thermomechanical simulation of hot isostatic pressing of metal powder, Eq. (6) is integrated with respect to time in a time interval Δt, which can be linked to the punch speed, or the increment of prescribed powder displacement. Assuming that T_n is known at time t_n, the temperature T_{n+1} must be evaluated at t_{n+1} while marching the solution forward at time $t_{n+1}=t_n+\Delta t$. The nonlinearity in the heat conduction FE equation arises from the matrix $\mathbf{C}$, in which the density of powder increases by time and the thermal conductivity $\mathbf{H}$ is dependent on the density of powder. The temperature evaluation in Eq. (6) is treated in a consecutive manner where the mechanical equilibrium system is first fulfilled so that the matrices $\mathbf{C}$ and $\mathbf{H}$ can be obtained at time t_n where the initial temperature is given at the first time step as T_0. The total computational process for the thermomechanical analysis proceeds with the following steps:

Step 1. *Initializing* the values of time, domain, and temperature by t_0, Ω_0, and T_0

Step 2. *Mechanical analysis*; considering the values of displacement, volumetric strain, and relative density at time t_n by $\overline{\mathbf{u}}_n$, $(\varepsilon_v)_n$, and ρ_n, we obtain the values of displacement, volumetric strain, and relative density at time t_{n+1} using the nonlinear mechanical analysis

Step 3. *Thermal resolution*; evaluate the matrices $\mathbf{C}$ and $\mathbf{H}$ based on the values obtained from the mechanical analysis, and obtain the value of temperature T_{n+1} at t_{n+1} by solving Eq. (6)

Step 4. *Updating the variables*; determine the internal variables at time steps t_{n+1}, including the displacement field $\overline{\mathbf{u}}_{n+1}=\overline{\mathbf{u}}_n+\Delta\overline{\mathbf{u}}$, the vector of strain $\boldsymbol{\varepsilon}_{n+1}=\boldsymbol{\varepsilon}_n+\Delta\boldsymbol{\varepsilon}$, and the relative density as $\rho_{n+1}=\rho_n/[1+(\varepsilon_v)_n]$

Step 5. *Go to step 2*; in order to perform the numerical analysis at the next increment

4 Constitutive model for metal powder

4.1 Cap plasticity model

The mechanical behavior of powders involves several interacting micromechanical processes. Firstly, at low pressure, particle sliding occurs leading to particle re-arrangement. The second stage involves both elastic and plastic deformation of the particles via their contact areas leading to geometric hardening (i.e., plastic deformation and void closure). Lastly, at very high pressure, the flow resistance of the material increases rapidly due to material strain hardening. Therefore, it is necessary that the constitutive model of powder captures various behaviors of the compaction process. A number of constitutive models have been developed for the compaction of powders over the last three decades, including the micromechanical model by Ransing et al. [19] and Martin et al. [20] and the macromechanical model by Khoei and Lewis [21] and Gasik and Zhang [22]. It was experimentally demonstrated by Gu et al. [23] that the constitutive modeling of granular and frictional materials can be utilized to construct suitable phenomenological constitutive models, which capture the major features of the response of initially loose powders to the complex deformation processing histories encountered in the manufacture of engineering components by powder metallurgy techniques. It was illustrated by Lewis and Khoei [24] and Chtourou et al. [25] that a two-mechanism model, such as Drucker–Prager or Mohr–Coulomb and elliptical cap models, which are widely used for geological materials and exhibit pressure-dependent behavior can be applied for modeling the behavior of powder materials. These models consist of two yield surfaces: a "distortion surface" which controls the ultimate shear strength of materials and a "cap" surface which captures the hardening behavior of materials [26, 27].

In order to describe the powder behavior during the compaction process, an appropriate constitutive model is employed based on the double-surface cap plasticity, as shown in Fig. 1. The yield surface of this elastoplastic model has a moving cap, intersecting the hydrostatic loading line, whose position is a function of plastic volumetric strain. The main features of the cap model include a failure surface and an elliptical yield cap which closes the open space between the failure surface and the hydrostatic axis. The cap surface expands in the stress space according to a specified hardening rule. The functional forms for these surfaces are as follows:

$$f_1=\sqrt{J_{2D}}-\theta J_1+\gamma e^{-\beta J_1}-\alpha=0 \tag{8}$$

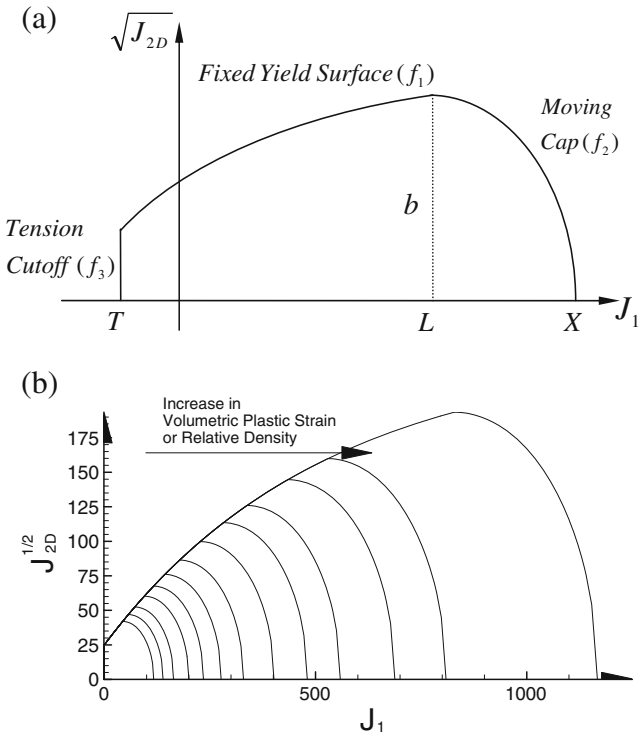

Fig. 1 The double-surface cap plasticity: **a** definition of yield surfaces and **b** the expansion of moving cap surface with increasing the volumetric plastic strain, or relative density

$$f_2 = R^2 J_{2D} + (J_1 - L)^2 - R^2 b^2 = 0 \tag{9}$$

$$f_3 = J_1 - T = 0 \tag{10}$$

where J_1 and J_{2D} are the first invariant of stress tensor and second invariant of deviatoric stress tensor, respectively. α, β, γ, and θ are the parameters of fixed yield surface f_1, which controls the deviatoric stress limits, and for the numerical examples presented in Section 5 are given in Table 1. The fixed yield surface f_1 is defined by an exponential function and in reality is consist of two different Drucker–Prager yield surfaces. The cap yield surface f_2 is an elliptical function, with R denoting the ratio of two elliptical cap's diameters. The function f_3 indicates the tension cutoff zone, with T denoting the material's tension limit.

Table 1 The material parameters for the cap plasticity model

Fixed yield surface parameters	Cap parameters	Tension cutoff
α=225 MPa	R=1.75	T=−0.3 MPa
β=0.002 MPa^{-1}	D=0.005 MPa	
γ=200 MPa	W=0.34	
θ=0.008	X_0=1 MPa	

Table 2 The elastic properties for 304 stainless steel

Shear modulus at 300°K	G_0=8.1×10^4 MPa
Melting point, T_m (K)	T_m=1,810°K
Temperature dependence of modulus	$\frac{T_m}{G_0}\frac{dG}{dT} = 0.85$

$G_m = G_0\left(1 - \frac{T-300}{G_0}\frac{dG}{dT}\right)$, $\nu_m = 0.27$

The hardening rule for moving cap is related to the volumetric plastic strain ε_v^p as

$$X(\kappa) = X\left(\varepsilon_v^p\right) = \frac{-1}{D}\ln\left(\frac{1-\varepsilon_v^p}{W}\right) + X_0 \tag{11}$$

where D and W are material parameters and X_0 refers to the position of initial cap surface. The plastic hardening/softening modulus H is zero for f_1 and f_3. Figure 1b shows how the cap yield surface grows with densification due to increase of the volumetric plastic strain.

4.2 Temperature-dependent cap plasticity model

In hot compaction of metal powder, it is of great importance to use realistic equations since these equations mainly determine the validity of simulation. Although the phenomenological approach based on experimental data has been proved to be more efficient, the experimental tests performed by industrial powders are often difficult to operate due to the required conditions of pressure (about 100 MPa) and temperature (up to 1,200°C). Thus, the relevant physically based models are necessary to describe the constitutive behavior of metal powders in hot isostatic pressing conditions. The final shape of HIPed component depends strongly

Table 3 The variations of yield stress (MPa) with temperature (°K) for 304 stainless steel at various volumetric strains

Volumetric strain (ε_v)	293 K	673 K	1,073 K	1,273 K	1,473 K
0	314	162	120	45	25
0.022			150	60	25
0.05		278			25
0.064			178		25
0.1		353	195	78	25
0.2	729	437	227	86	25
0.3	906		241	87	25
0.4	1,039	534			25
0.45	1,077				25
0.5	1,099		257	83	25
0.6		583			25
0.7			266	78	25

Table 4 The thermal properties for 304 stainless steel

T (°K)	k (W m^{-1} K)	c (J kg^{-1} K)
293	15.9	551
473	17.6	
477		591
700		586
811		598
922		576
973	22.3	
1,255		637

Activation energy $Q=2.8\times10^5$ J mol^{-1}. Gas constant $R=8.31434$ J K^{-1} mol^{-1}

on the HIP schedule used, i.e., on the history (or time variation) of the applied heat and pressure before their final values are reached. In fact, the process can be divided into three steps, in which during the first step a specified amount of powder is compacted by increasing the temperature. The compaction process starts at room temperature and usually increases linearly in accompany with inserting pressure by punch movements. At the end of this step, the powder mass has achieved a density of 50–70 % of the fully dense metal. During the second step, the component obtained from the first step is compacted without increasing the temperature where the temperature is kept fix; however, punch movements and densification of the powder continue. Finally, during the third step, the temperature usually decreases linearly and the punch movements and densification of the powder continue. At the end of this step, the final product gains a complete filling of the die cavity, and these further result in full densification of the part achieving relative density equal to 0.9–1. The highest temperature required for this process depends on the type of powder and its application, but typical values stand the temperature ranging from 500 to 1,300°C.

In order to implement the temperature effect into the cap plasticity model described in preceding section, the hardening rule (Eq. 11) is modified by taking the temperature and the thermal stresses into the model, which has a major influence on the strain rate. To model the powder behavior at high temperature, an increasing power law is implemented in the cap plasticity, in which the power-law breakdown regime is associated with a transition from dislocation climb dominated flow to the dislocation glide dominated flow. Various empirical relationships have been proposed to accommodate both the power law and the exponential dependence of strain rate on stress. In order to obtain an optimum fit to experimental results, a modified hyperbolic equation is employed for the temperature-dependent hardening rule of moving cap as

$$X(\kappa)=X\left(\varepsilon_v^p,T\right)=\frac{AB}{T}\left[\frac{-1}{D}\ln\left(1-\frac{\varepsilon_v^p}{W}\right)+X_0\right]\exp(Q/(RT)) \tag{12}$$

where A, B, and Q are material parameters, R is the universal gas constant, and T is the absolute temperature. In above hardening rule, parameters A and Q are pre-exponential temperature factors and activation energy, respectively, and B is a constant set to 7.0482×10^{-4} for metal powders. According to the experiments performed on stainless steel [28], A is assumed as the temperature-dependent function defined by

$$A=\frac{C}{T^m}+D \tag{13}$$

where C, D, and m are the material constants and for metal powders are given in Tables 2, 3, and 4. The temperature effect

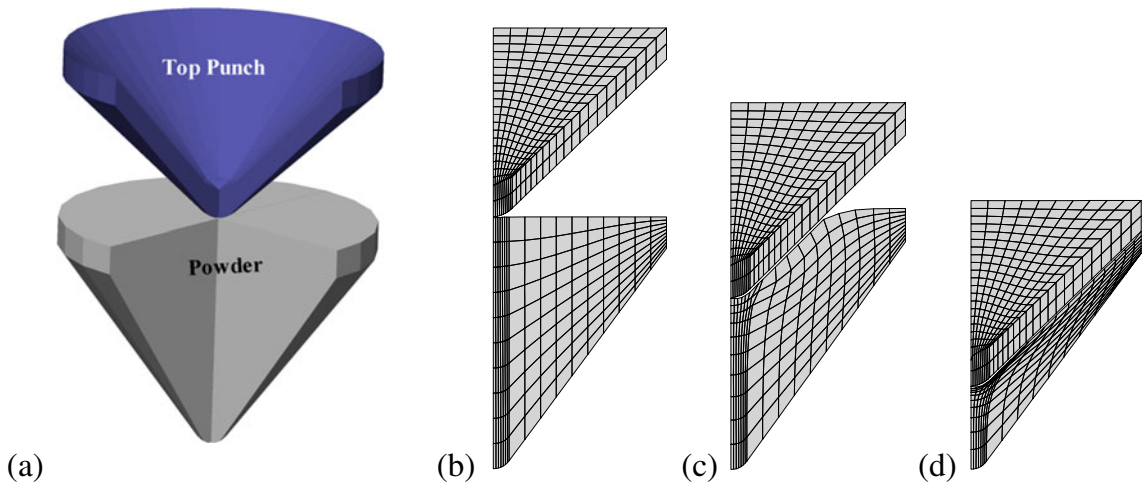

Fig. 2 A conical-shaped charge liner: **a** geometry and boundary conditions, **b** initial FE mesh, **c** the half stage of compaction, and **d** the final stage of compaction

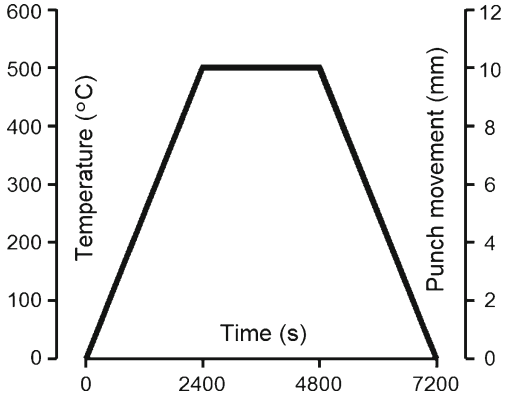

Fig. 3 The prescribed temperature and punch movement during the compaction process

on the strain rate is essentially represented by an Arrhenius-type expression. For absolute temperatures above $T \approx 0.6T_m$, with T_m denoting the melting temperature of material, the value of the activation energy Q does not vary with the temperature and stress; however, at lower temperatures, it becomes temperature sensitive.

5 Numerical simulation results

In order to illustrate the efficiency and applicability of proposed computational algorithm, two practical examples are presented numerically. The first example is the hot compaction process of a shaped charge liner chosen to demonstrate the capability of proposed temperature-dependent cap plasticity in the large FE deformation of thermomechanical simulation. The simulation is performed using the nonlinear FE model combined with the heat transfer analysis in a nonlinear finite element code. The second example is the shape optimization of an automotive component chosen to demonstrate the design optimization of an industrial automotive component in the cold and warm compaction processes in the framework of the GA technique.

Both numerical examples have been solved under the displacement control condition by increasing the punch movement and predicting the die-pressing forces at different displacements. The distribution of stress, relative density, and temperature contours are presented at different generations of optimization process. The experimental data are gained from a set of compaction experiments on an iron-based powder performed by Doremus et al. [29]. The material parameters of cap plasticity model are given in Table 1 [30], and the thermal properties of iron powder are summarized in Tables 2, 3, and 4 [28]. The initial relative density is $\overline{\rho}_0 = 0.4$. The variation of the Young modulus with relative density for iron powder is assumed as $E = 3640\overline{\rho}^{3.9}$, with $\overline{\rho}$ denoting the relative density [31]. In the FE simulations, the tools are modeled as rigid bodies, since the elastic deformation of the tools has only an insignificant influence on the density distribution in the green component.

5.1 A conical-shaped charge liner

The first example is of a shaped charge liner, which is extensively used for civilian oil and steel sectors in geophysical prospecting, mining, and quarrying. Most liners used in the civilian sector have a conical shape and are often made from a mixture of different metallic powders. This component was modeled by Gu et al. [23] and Khoei et al. [32] using the cold compaction simulation. In the present

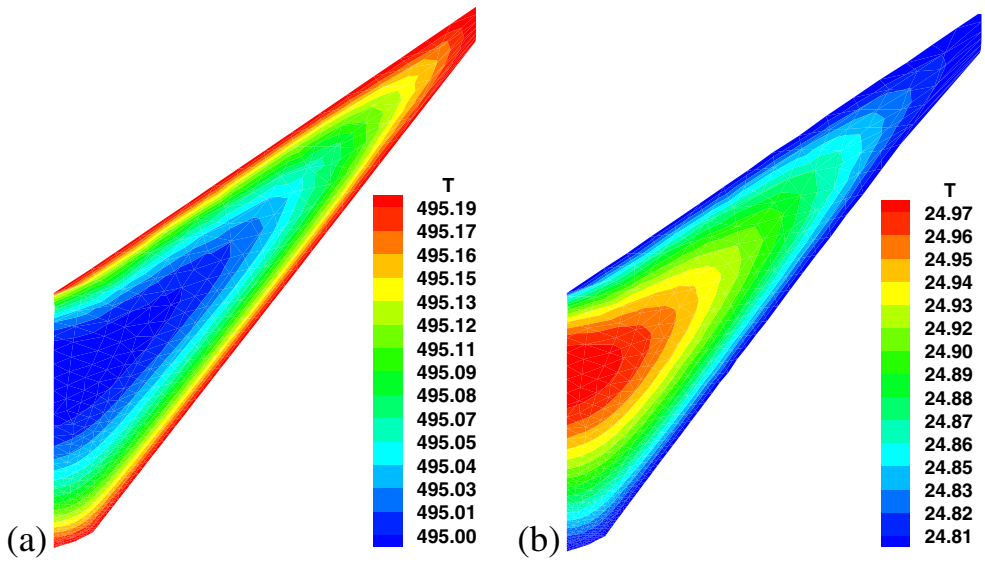

Fig. 4 The distribution of temperature for a shaped charge liner at the end of **a** first stage and **b** final stage

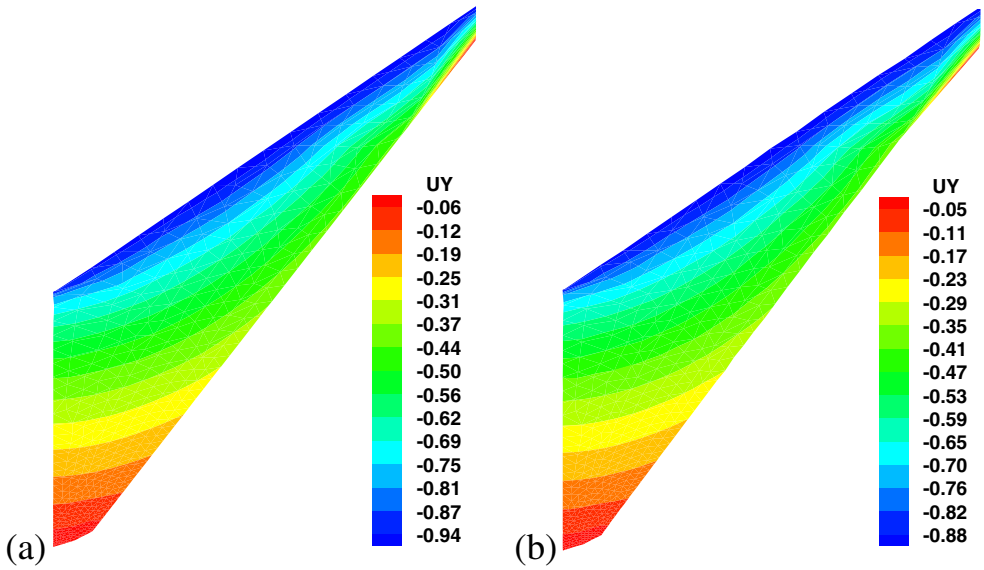

Fig. 5 The distribution of vertical powder movement for a shaped charge liner at the end of **a** first stage and **b** final stage

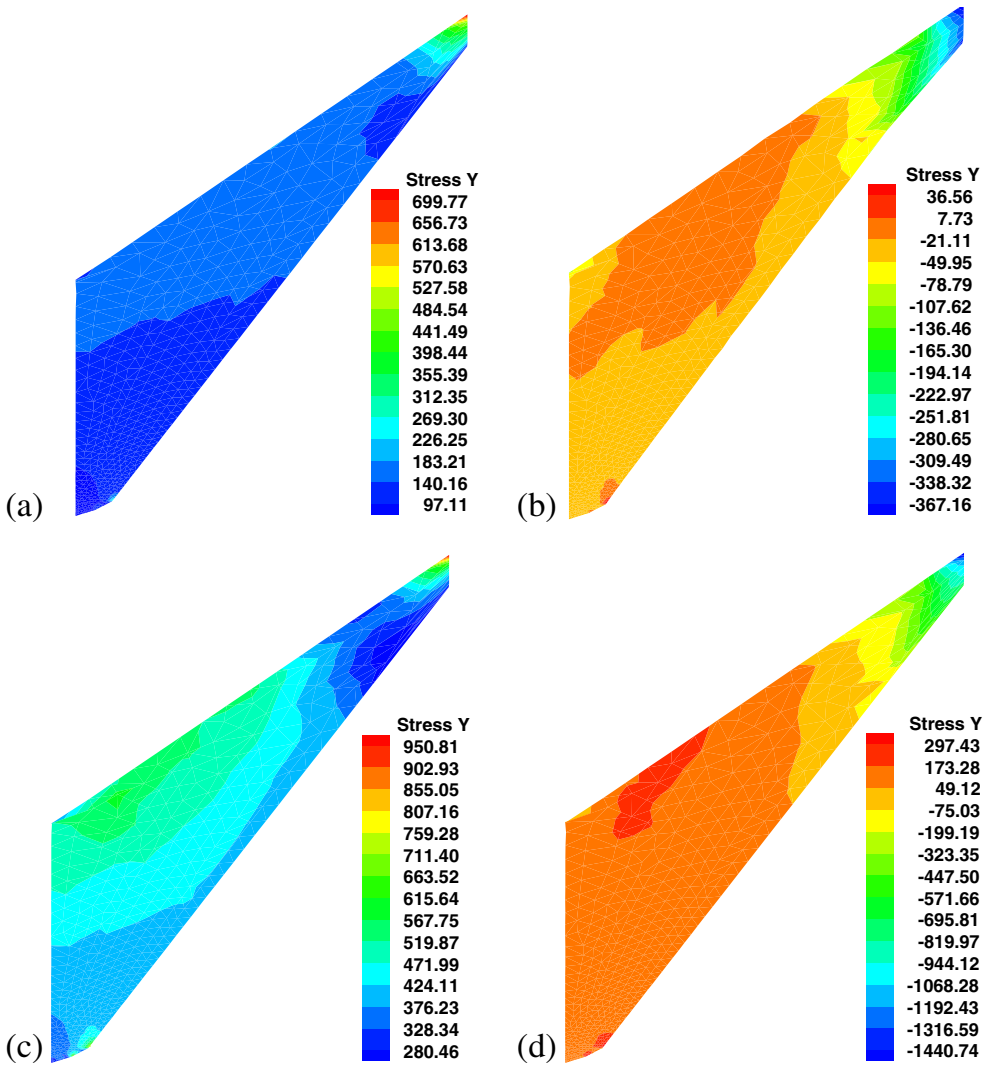

Fig. 6 The stress σ_y contours at the end of first and final stages of process: **a**, **b** hot pressing and **c**, **d** cold pressing

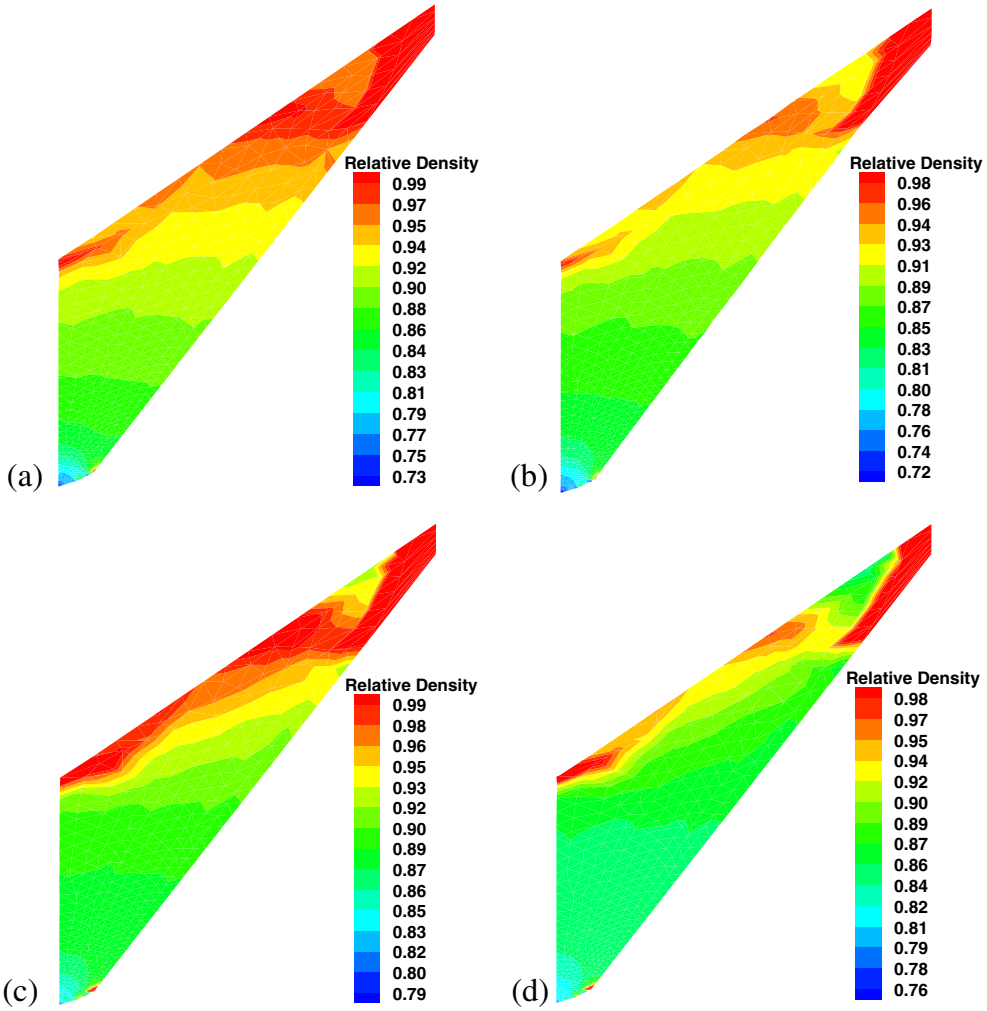

Fig. 7 The relative density contours at the end of first and final stages of process: **a**, **b** hot pressing and **c**, **d** cold pressing

study, the hot-forming simulation is presented based on the large FE deformation of thermomechanical analysis. The schematic of the process to form a conical-shaped charge liner from iron powder along with the geometry, initial, and deformed FE meshes of powder and punch is presented in Fig. 2. The loading characteristics are achieved by the use of prescribed nodal displacements for the top punch movement. The simulation has been performed using the remaining pressing distance of 10 mm from top.

The hot process of powder die pressing is performed in three stages, as shown in Fig. 3. At the first stage, the top punch movement is gradually applied while the temperature between the powder and tools raises from 20 to 500°C, in which at the end of first stage the temperature of boundaries of component is 500°C and the punch movement is 10 mm. In the second stage, the value of temperature is kept at 500°C and the top punch position is fixed at 10 mm from the top. At the final stage, the top punch is gradually removed from the component and simultaneously the temperature of boundaries decreases from 500 to 20°C, as shown in Fig. 3. In Fig. 4, the contours of temperature distribution are shown at the end of first and final stages of compaction process. Also plotted in Fig. 5 are the contours of vertical displacement at two stages. The distribution of normal stress and relative density contours are shown in Figs. 6 and 7 at the end of first and final stages of compaction process, respectively. In these figures, the contours of final stress and relative density distributions obtained by the hot compaction process are compared with those predicted by the cold compaction process. The results of density contours demonstrate that the uniform density distribution can be observed for both the hot and cold compaction processes. However, the mean value of stress in cold compaction process is almost three times of hot compaction process.

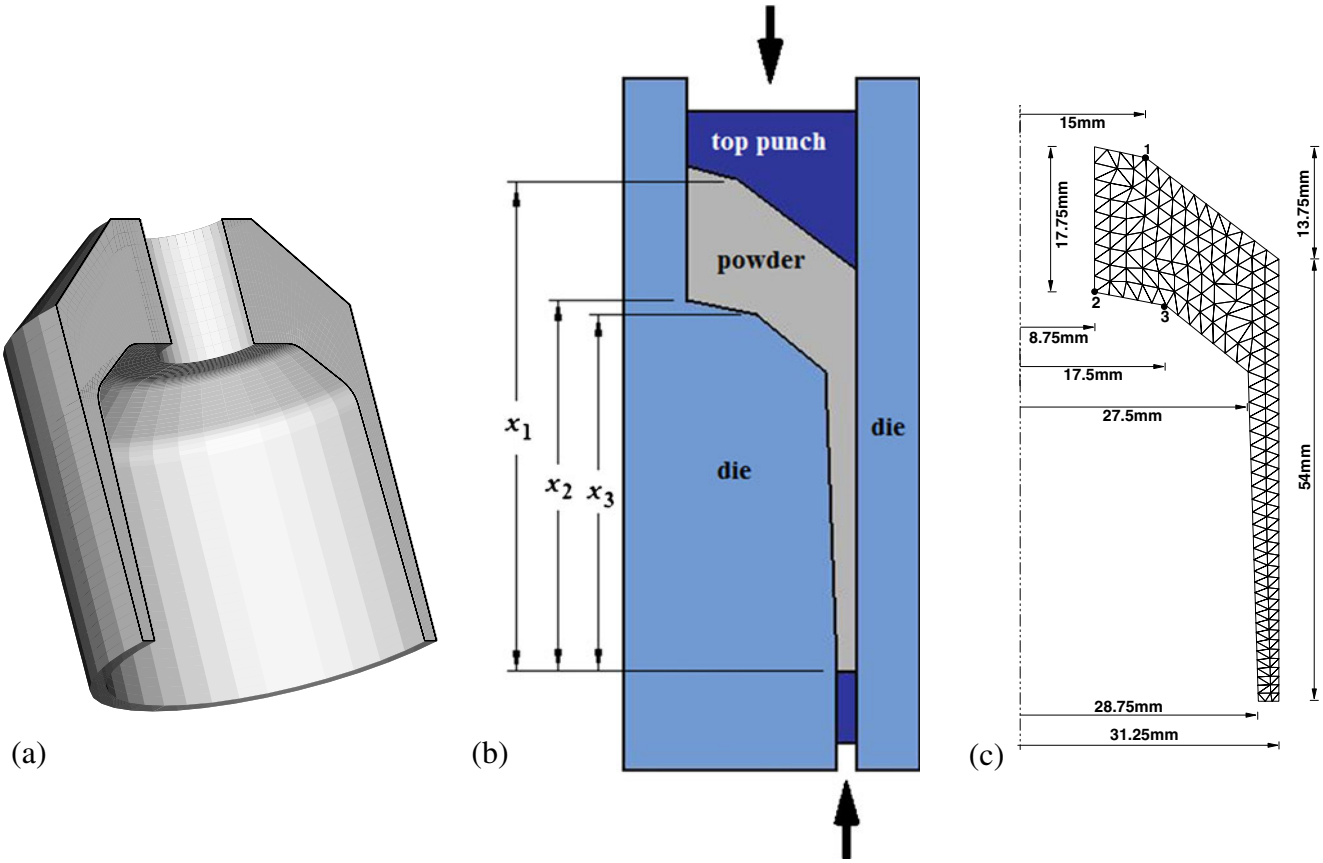

Fig. 8 **a** An automotive component, **b** the problem description, and **c** the geometry and boundary conditions (the FE mesh using 314 elements)

5.2 An automotive component

The next example is of an axisymmetric automotive part which is compacted from iron powder with a mechanical press and a multi-platen die set. This practical example is chosen to present the capability of proposed computational algorithm in shape optimization of an automotive component in the cold and warm compaction processes. The cold compaction process of this component was investigated experimentally by Shen et al. [33] and numerically by Khoei et al. [32]. The shape of powder together with the die and punches in their position before compaction are presented in Fig. 8. On the virtue of symmetry, the automotive part is analyzed employing an axisymmetric FE mesh. The compaction is employed by means of the action of two punches from the top and bottom simultaneously. The simulation has been performed using the remaining pressing distance of top punch 7.5 mm and bottom punch of 20 mm. The hot compaction process is performed in three stages, as shown in Fig. 9. At the first stage, the top and bottom punches move simultaneously to 7.5 and 20 mm, respectively, and at the same time, the temperature between the powder and tools raises from 20 to 500°C. In the second stage, the temperature is kept at 500°C and the top and bottom punch positions are fixed at 7.5 and 20 mm, respectively. At the final stage, the top and bottom punches are gradually removed from the component and simultaneously the temperature of boundaries decreases from 500 to 20°C.

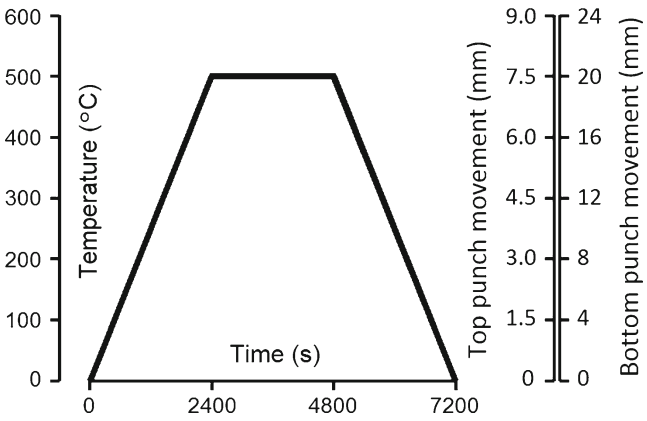

Fig. 9 The prescribed temperature and punch movement during the compaction process

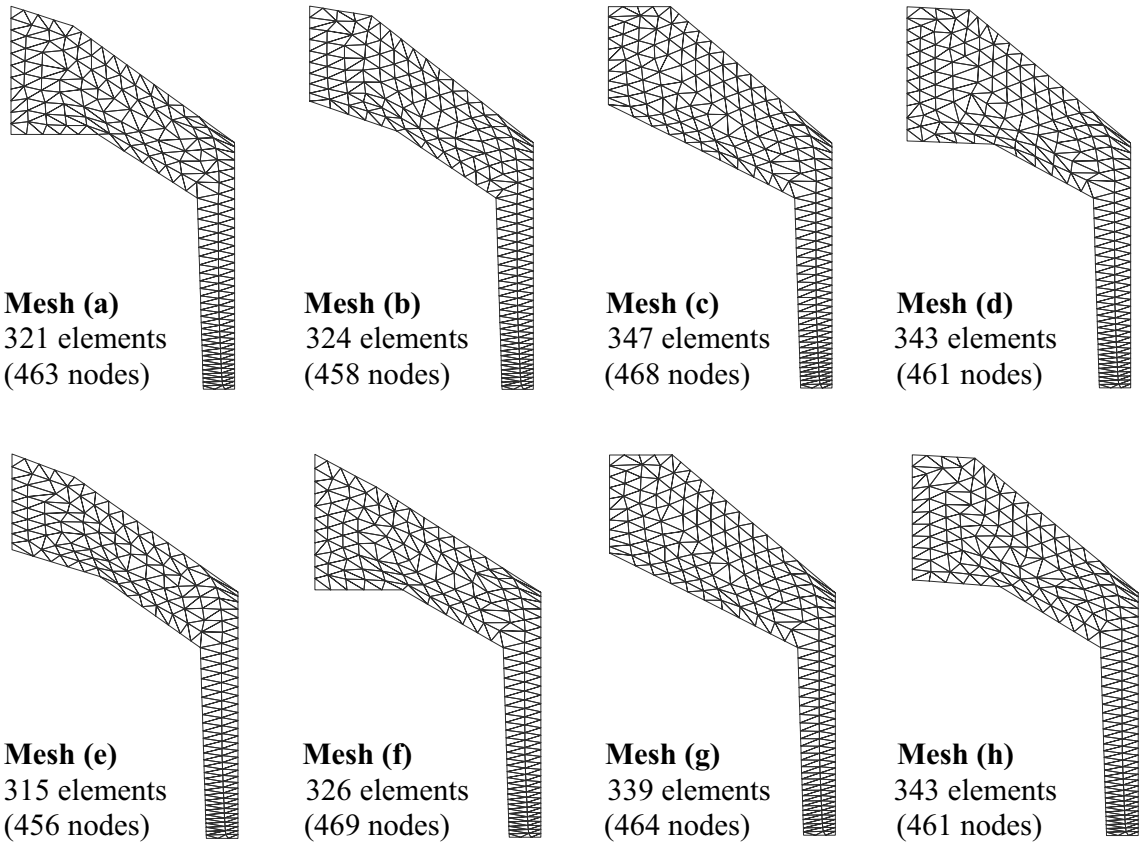

Fig. 10 The deformed FE meshes of compacted component at four generations of optimization process: **a**–**d** hot compaction process and **e**–**h** cold compaction process

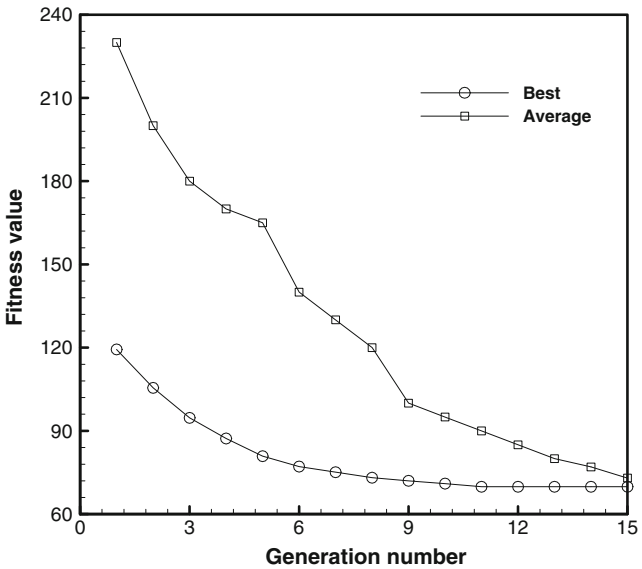

Fig. 11 The variations of the objective function with the number of generation for the best and average generations in the hot compaction process

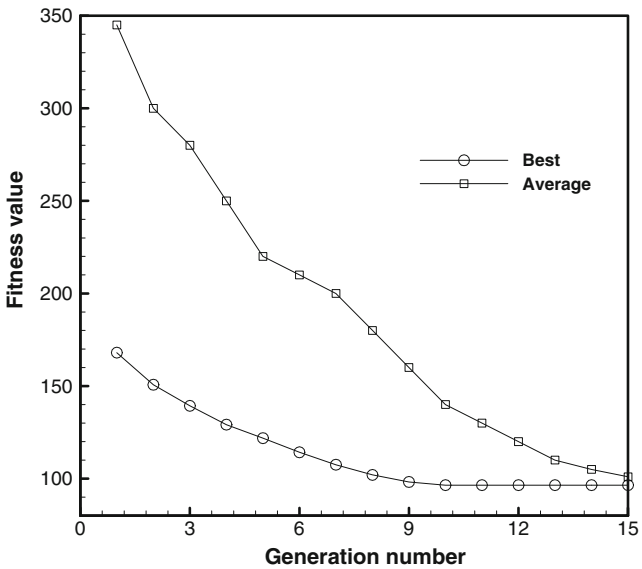

Fig. 12 The variations of the objective function with the number of generation for the best and average generations in the cold compaction process

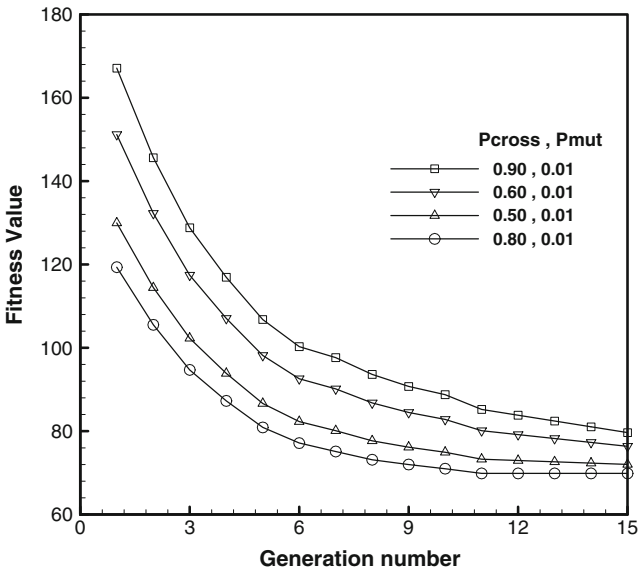

Fig. 13 The variations of the objective function with the number of generation for the mutation rate of 0.01 at various rates of crossover in the hot compaction process

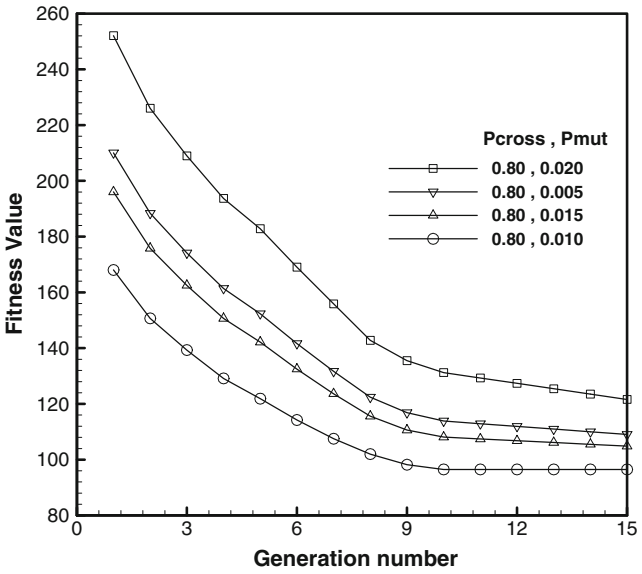

Fig. 15 The variations of the objective function with the number of generation for the crossover rate of 0.8 at various rates of mutation in the hot compaction process

The objective of proposed die pressing is to design the preform die shape so that, after the final compaction, the required final product is obtained without defects. The shape of the geometry of free surface of the preform workpiece is considered as the unknown design variables with three control points, as shown in Fig. 8. The optimization scheme is used to optimize the difference between the maximum and minimum values of stress on the final compacted component. The objective function for this example is as follows:

$$\text{Minimize} \quad f(x_1, x_2, x_3) = |\sigma_{\max} - \sigma_{\min}| \tag{14}$$

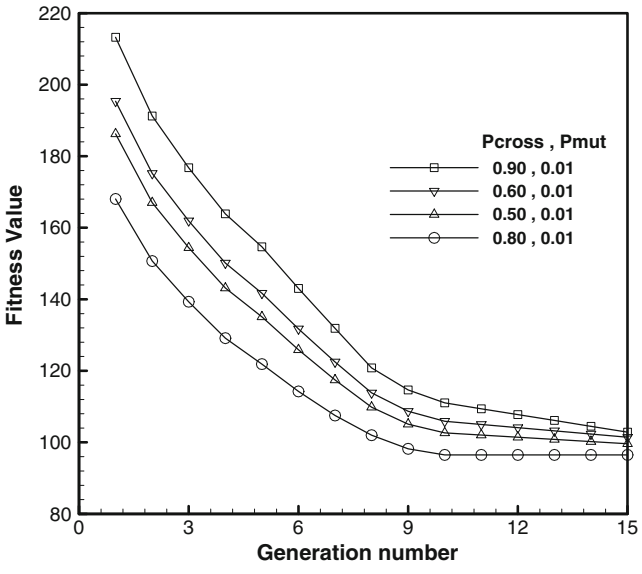

Fig. 14 The variations of the objective function with the number of generation for the mutation rate of 0.01 at various rates of crossover in the cold compaction process

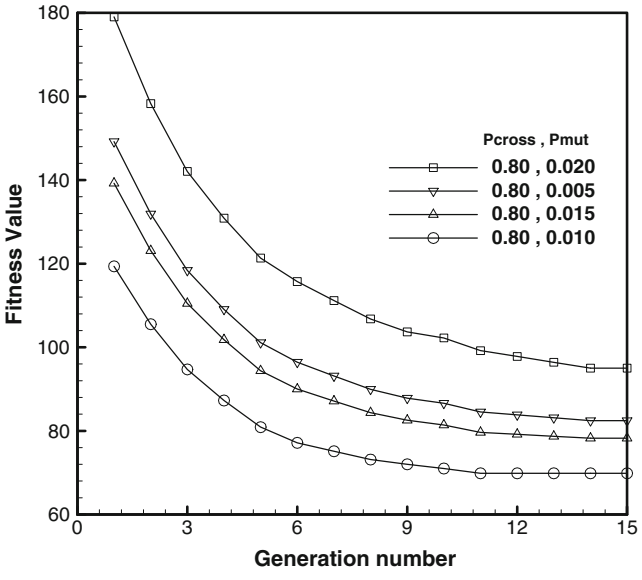

Fig. 16 The variations of the objective function with the number of generation for the crossover rate of 0.8 at various rates of mutation in the cold compaction process

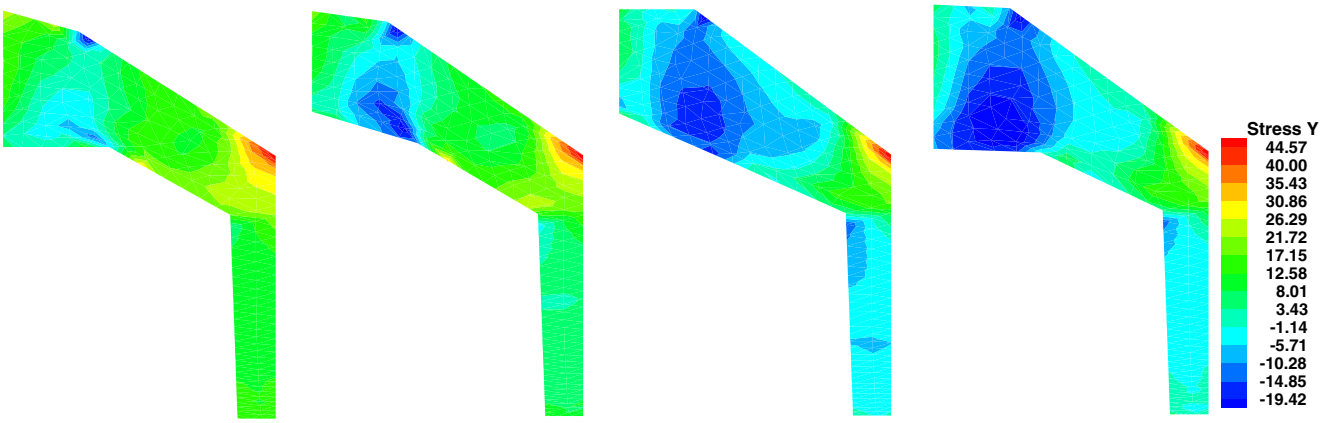

Fig. 17 The normal stress σ_y contours using the hot compaction process at four generations of optimization process

with the constraints of $62.5 \leq x_1 \leq 67.5$, $45.0 \leq x_2 \leq 50.0$, $45.0 \leq x_3 \leq 50.0$, $x_2 - x_3 \geq 0.0$, and $x_2 - 1.875x_3 \leq -35.2$. The first three constraints are applied to control the geometry of the top and bottom punches and the last two constraints to control the slope of bottom punch surfaces.

The optimization process for this example is performed using the genetic algorithm technique, as described in Section 2. The initial population is generated randomly using 50-string based on three control points x_1, x_2, and x_3. To calculate the fitness and reproduction, the numerical simulation is performed for each string by using the 2D axisymmetric FE mesh of three-noded elements. For each string, the value of objective function is calculated at the end of compaction. The process of reproduction is applied according to the fitness function to copy the individual string. The reproduction operator is implemented in the algorithmic form based on a roulette wheel where each individual is represented by a space that proportionally corresponds to its fitness. It has been observed that the evolutionary process is converged after 15 generations. The optimal design variables for three control points corresponding to the hot compaction process is obtained as $X_3{}^T$=[67.5, 46, 45] and the cold compaction process as $X_6{}^T$=[67.5, 46, 45]. Obviously, the hot and cold compaction processes result in similar design variables, as can be observed in Fig. 10d, h.

In Fig. 10, the deformed FE meshes of compacted component are presented at four generations of optimization process using the hot and cold compaction processes. The optimal preform shapes of final component obtained in Fig. 10d, h are similar to that measured experimentally by Shen et al. [33]. In Figs. 11 and 12, the variations of the objective function are plotted with the number of generation for the best and average generations using the hot and cold

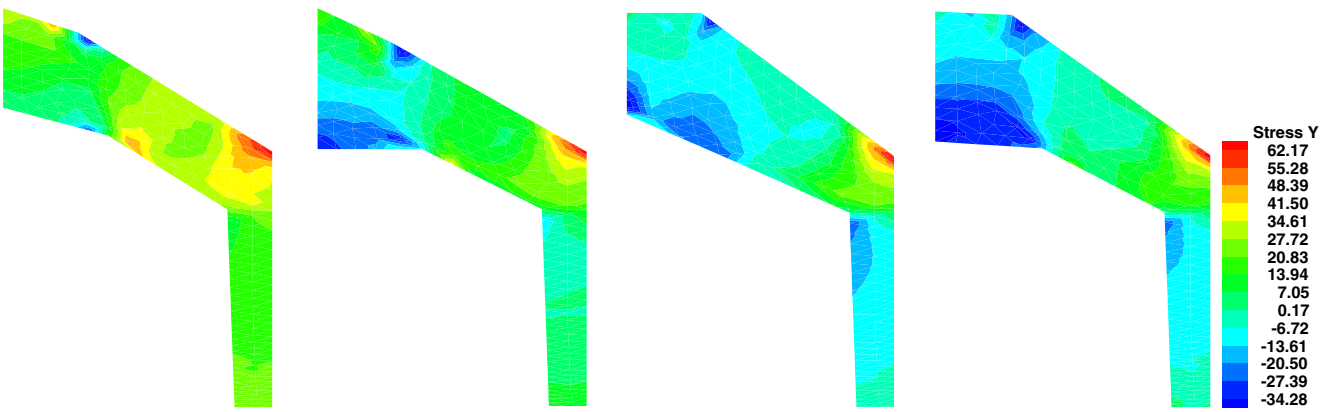

Fig. 18 The normal stress σ_y contours using the cold compaction process at four generations of optimization process

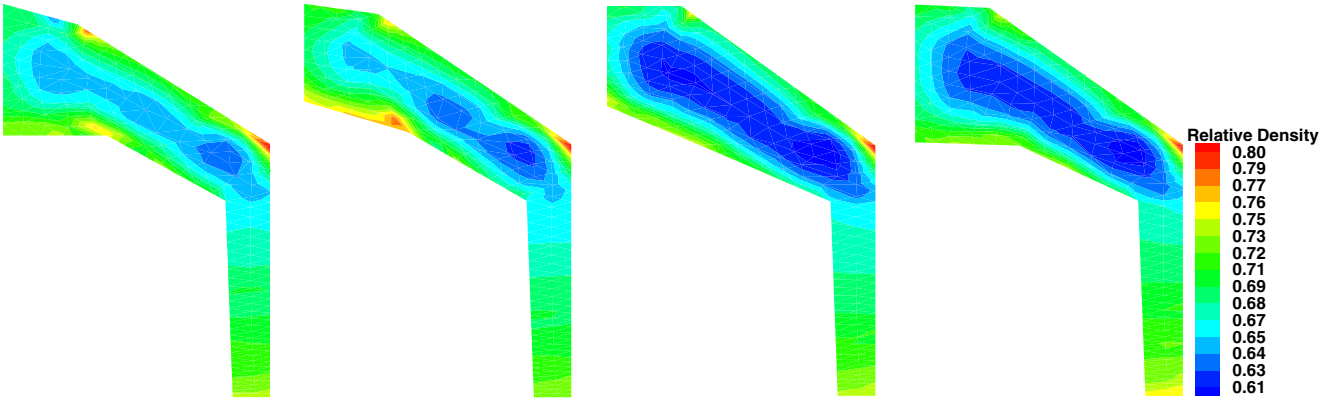

Fig. 19 The relative density distributions using the hot compaction process at four generations of optimization process

compaction processes. In order to evaluate the optimum values of crossover and mutation, the optimization process is performed for various rates of crossover in the range of [0.5–0.9] and different rates of mutation in the range of [0.005–0.02]. In Figs. 13 and 14, the variations of the objective function with the number of generation are plotted for the mutation rate of 0.01 at various rates of crossover, i.e., 0.5, 0.6, 0.8, and 0.9 in the hot and cold compaction processes. Obviously, the optimal design variables can be obtained for the crossover rate of 0.8. In Figs. 15 and 16, the variations of the objective function with the number of generation are plotted for the crossover rate of 0.8 at various rates of mutation, i.e., 0.005, 0.01, 0.015, and 0.02 in the hot and cold compaction processes. Clearly, it can be observed that the optimum value of mutation is equal to 0.01. Finally, on the basis of optimum values of the crossover rate of 0.8 and the mutation rate of 0.01, the distribution of normal stress σ_y contours are presented in Figs. 17 and 18 at four generations of optimization process using the hot and cold compaction processes, respectively. Also plotted in Figs. 19 and 20 are the predicted relative density distributions at four generations of optimization process using the hot and cold compaction processes. At the end of compaction, the relative density contour shows the highest density values at the bottom punch surface and the top-right corner for the optimal component.

6 Conclusion

In the present paper, an optimization algorithm was presented for the hot powder forming process based on the genetic algorithm approach. The goal of optimization was to eliminate the workpiece defects that may arise during the powder compaction process. The genetic algorithm operator was used to increase the efficiency of the search algorithm

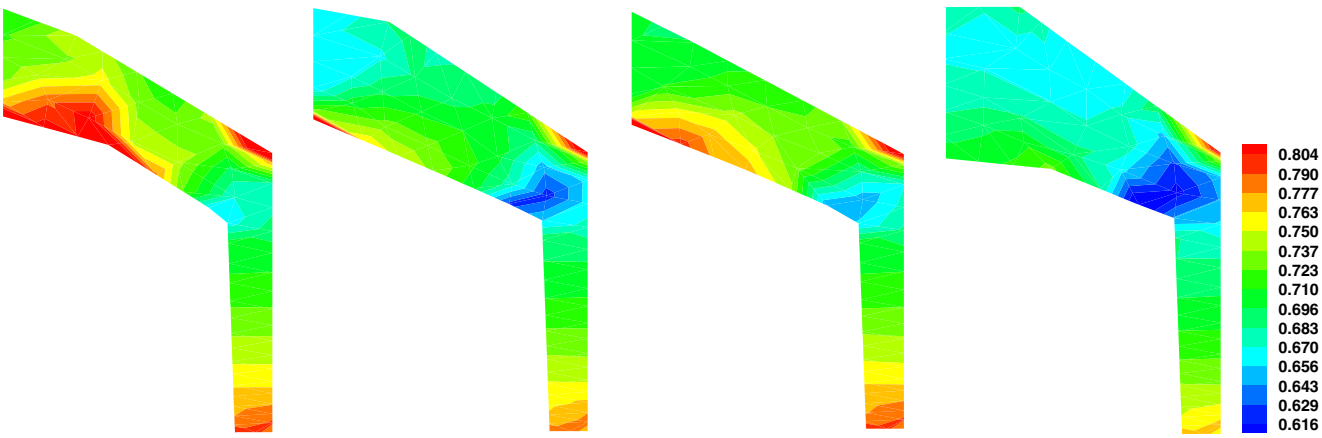

Fig. 20 The relative density distributions using the cold compaction process at four generations of optimization process

and to produce an optimal design. The coupled thermomechanical analysis of hot isostatic pressing was employed based on the large deformation formulation, temperature-dependent cap plasticity model, and frictional contact algorithm. A modified cap plasticity model considering the temperature effects was used in numerical simulation of nonlinear behavior of metal powder. Finally, numerical examples are analyzed to demonstrate the feasibility of proposed optimization algorithm for designing powder components in the hot-forming process of powder compaction.

Acknowledgment The authors are grateful for the research support of the Iran National Science Foundation (INSF).

References

1. Goldberg DE (1989) Genetic algorithms in search optimization and machine learning. Addison-Wesley, Reading
2. Khoei AR, Lewis RW (1998) Finite element simulation for dynamic large elasto-plastic deformation in metal powder forming. Finite Elem Anal Des 30:335–352
3. Haggblad HA, Oldenburg M (1994) Modeling and simulation of metal powder die pressing with use of explicit time integration. Model Simul Mater Sci Eng 2:893–911
4. Brandt J, Nilsson L (1999) A constitutive model for compaction of granular media with account for deformation induced anisotropy. Mech Coh Fric Mater 4:391–418
5. Keshavarz SH, Khoei AR, Khaloo AR (2008) Contact friction simulation in powder compaction process based on the penalty approach. Mater Des 29:1199–1211
6. Jinka AGK, Lewis RW (1994) Finite element simulation of hot isostatic pressing of metal powders. Comp Meth Appl Mech Eng 114:249–272
7. Svoboda A, Haggblad HA, Nasstrom M (1996) Simulation of hot isostatic pressing of metal powder components to near net shape. Eng Comput 13:13–37
8. Jinka AGK, Bellet M, Fourment L (1997) A new 3D finite element model for the simulation of powder forging processes: application to hot forming of PM connecting rod. Int J Numer Meth Eng 40:3955–3978
9. Khoei AR, Keshavarz Sh, Biabanaki SOR (2010) Optimal design of powder compaction processes via genetic algorithm technique. Finite Elem Anal Design 46:843–861
10. Zhao G, Wright E, Grandhi RV (1997) Preform die shape design in metal forming using an optimization method. Int J Numer Meth Eng 40:1213–1230
11. Antonio CAC, Dourado NM (2002) Metal forming process optimization by inverse evolutionary search. J Mater Proc Tech 121:403–413
12. Sousa LC, Castro CF, Antonio CAC, Santos AD (2002) Inverse methods applied to industrial forging processes. Int J Form Proc 4:463–479
13. Holland JH (1992) Adaptation in natural and artificial systems. University of Michigan Press, USA
14. Michalewicz Z (1992) Genetic algorithms+data structures=evolution programs. Springer, Berlin
15. Roy S, Ghosh S, Shivpuri R (1997) A new approach to optimal design of multi-stage metal forming processes with micro genetic algorithms. Int J Mach Tool Manufact 37:29–44
16. Castro CF, Sousa LC, Antonio CAC, César de Sá J (2001) An efficient algorithm to estimate optimal preform die shape parameters in forging. Eng Comput 18:1057–1077
17. Amirjanov A (2006) The development of a changing range genetic algorithm. Comp Meth Appl Mech Eng 195:2495–2508
18. Khoei AR, Biabanaki SOR, Vafa AR, Yadegaran I, Keshavarz SH (2009) A new computational algorithm for contact friction modeling of large plastic deformation in powder compaction processes. Int J Solids Struct 46:287–310
19. Ransing RS, Gethin DT, Khoei AR, Mosbah P, Lewis RW (2000) Powder compaction modelling via the discrete and finite element method. Mater Des 21:263–269
20. Martin CL, Bouvard D, Shima S (2003) Study of particle rearrangement during powder compaction by the discrete element method. J Mech Phys Solids 51:667–693
21. Khoei AR, Lewis RW (1999) Adaptive finite element remeshing in a large deformation analysis of metal powder forming. Int J Numer Meth Eng 45:801–820
22. Gasik M, Zhang B (2000) A constitutive model and FE simulation for the sintering process of powder compacts. Comput Mater Sci 18:93–101
23. Gu C, Kim M, Anand L (2001) Constitutive equations for metal powders: application to powder forming processes. Int J Plasticity 17:147–209
24. Lewis RW, Khoei AR (2001) A plasticity model for metal powder forming processes. Int J Plasticity 17:1659–1692
25. Chtourou H, Gakwaya A, Guillot M (2002) Modeling of the metal powder compaction process using the cap model. Part II: numerical implementation and practical applications. Int J Solids Struc 39:1077–1096
26. Khoei AR, DorMohammadi H, Azami AR (2007) A three-invariant cap plasticity model with kinematic hardening rule for powder materials. J Mater Proc Tech 187:680–684
27. Hrairi M, Chtourou H, Gakwaya A, Guillot M (2011) Modeling the powder compaction process using the finite element method and inverse optimization. Int J Adv Man Tech 56:631–647
28. Frost HJ, Ashby MF (1982) Deformation-mechanism maps: the plasticity and creep of metals and ceramics. Pergamon, Oxford
29. Doremus P, Geindreau C, Martin A, Debove L, Lecot R, Dao M (1995) High pressure triaxial cell for metal powder. Powder Metal 38:284–287
30. Khoei AR, Azizi S (2004) Numerical simulation of 3D powder compaction processes using cone-cap plasticity theory. Mater Des 26:137–147
31. Khoei AR (2002) Numerical simulation of powder compaction processes using an inelastic finite element analysis. Mater Des 23:523–529
32. Khoei AR, Azami AR, Anahid M, Lewis RW (2006) A three-invariant hardening plasticity for numerical simulation of powder forming processes via the arbitrary Lagrangian–Eulerian FE model. Int J Numer Meth Eng 66:843–877
33. Shen WM, Kimura T, Takita K, Hosono K (2001) Numerical simulation of powder transfer and compaction based on continuum model. In: Mori K (ed) Simulation of materials processing: theory, methods and applications. Swets & Zeitlinger, Lisse, pp 1027–1032